European Journal of Soil Science, June 2007, **58,** 802–810 doi: 10.1111/j.1365-2389.2006.00870.x

Visualization of root growth in heterogeneously contaminated soil using neutron radiography

M. Menon[a], B. Robinson[a], S. E. Oswald[b], A. Kaestner[a], K. C. Abbaspour[c], E. Lehmann[d] & R. Schulin[a]

[a]*Institute of Terrestrial Ecology, Swiss Federal Institute of Technology (ETH), Universitatstrasse 16, 8092, Zurich, Switzerland*, [b]*Department of Hydrogeology, UFZ Centre for Environmental Research, Permoserstrasse 15, D-04318 Leipzig, Germany*, [c]*Swiss Federal Institute for Aquatic Science and Technology (EAWAG), Ueberlandstrasse 133, PO Box 611, 8600, Duebendorf, Switzerland and* [d]*Paul Scherrer Institute (PSI), 5232, Villigen, Switzerland*

Summary

We used neutron radiography (NR), a non-invasive and *in situ* technique, to study living plant roots in soil. Plant roots have a larger water content than their unsaturated surrounding media. As water strongly attenuates a neutron-beam, NR can identify root structures in detail. We investigated the use of NR to visualize the root growth of lupin in quartz sand and in a loamy sand field soil. Further experiments elucidated the root growth of lupin in the loamy sand heterogeneously contaminated with 10 and 20 mg kg^{-1} boron (B) and 100 mg kg^{-1} zinc (Zn). We obtained high-quality images of root growth dynamics in both media with a resolution range of 110–270 μm. The images with quartz sand revealed fine structures such as proteoid roots that are difficult to locate *in situ* by other methods without destruction of the soil. Though quartz sand provided excellent visibility of roots, it proved to be a poor medium for growing plants, probably because of its bulk density (1.8 Mg m^{-3}). The images with field soil showed normal root growth with slightly less contrast than the quartz sand. The poorer contrast was due to the greater neutron interaction with soil water and soil organic matter. In the heterogeneously contaminated soil, root growth was significantly reduced in the contaminated part of the soil in all B and Zn treatments. This study shows that NR has potential as a non-invasive method to investigate root growth over time as well as the response of roots to various abiotic stress factors.

Introduction

Roots are the hidden half of terrestrial plants. Our understanding of root systems is limited by the difficulty of observing root growth and activity without destruction of the surrounding soil. The development of *in situ* and non-invasive techniques for root measurement would alleviate these difficulties. At present, the non-destructive techniques available for measuring root growth are: (a) monitoring by means of minirhizotrons, which are transparent plastic tubes inserted into the ground to view the roots using a video camera; (b) X-radiography (Gregory *et al*., 2003; Pierret *et al*., 2003); and (c) neutron radiography (Willatt & Struss, 1978; Willatt *et al*., 1978; Couchat *et al*., 1980; Furukawa *et al*., 1999). Although non-destructive, minirhizotrons have an invasive component (Majdi, 1996), while neutron radiography (NR) and X-radiography (X-ray) are complementary non-invasive imaging techniques. X-rays interact with the electronic shells of atoms, whereas neutrons interact with the nuclei of atoms. Therefore, neutron radiographs and X-radiographs show different characteristics of the imaged object. Both methods can provide two-dimensional images in transmission, such as in traditional medical X-ray imaging, or be used to perform three-dimensional tomography, as in the case of X-ray computer tomography (CT).

Radiography techniques (X-ray or NR) are based on the exponential law (similar to the Lambert–Beer law) of attenuation of radiation passing through matter (Kasperl & Vontobel, 2005):

$$I = I_0 \exp\left(-\Sigma_{\text{Sample}} d\right), \tag{1}$$

where I is the attenuated neutron flux (m^{-2} s^{-1}) after an incident neutron flux I_0 passes through a material of thickness d (m) with an attenuating constant Σ_{Sample} (m^{-1}), which is a characteristic of the material (not a summation). The quantity I represents an integer ranging from 0 to 65 535, which is a grey value proportional to the neutron flux.

As materials differ in their attenuating behaviour, a neutron beam passing through a sample provides information about

Correspondence: B. Robinson. E-mail: brett.robinson@env.ethz.ch
Received 1 February 2005; revised version accepted 3 August 2006

the composition and structure of the sample. Neutron radiography is a powerful tool for imaging water distribution in a sample, as hydrogen has a relatively large Σ value. The volumetric water content of plant roots generally ranges between 70 and 95%, while that of soils at field capacity usually ranges between 5 and 30%. This difference in water content provides sufficient contrast to distinguish roots from surrounding soil using NR. The neutron radiograph of a sample is a result of all the neutron attenuation processes occurring while the neutron beam penetrates a sample. Therefore, the visibility of roots depends on the thickness, water content or organic matter of the porous media. For example, dry quartz sand has greater neutron transmission than a dry soil of the same thickness and moisture content. Some workers used neutron radiography in the 1970s and 1980s to study early germination and root growth of corn (Couchat *et al*., 1980) and soybean (Willatt & Struss, 1978; Willatt *et al*., 1978). At that time low-resolution images were acquired using imaging plates or films and required much longer exposure times than modern CCD (charge coupled device) image capture methods.

Recently, NR has improved due to fast digital imaging and increased resolution. Digital imaging techniques that use a CCD camera combined with image processing tools yield quantifiable images with a resolution of about 100 μm. The required exposure time for such images is in the order of seconds. Images acquired using imaging plates or films required several minutes of exposure to the potentially damaging neutron beam. These advances open up the possibility of using this technique to study root system development in soils and simultaneously monitor soil moisture distribution.

Here we use neutron radiography to measure root growth in response to elevated concentrations of B and Zn in soil. Several investigations have shown, at large concentrations, that these essential elements inhibit plant root growth (Breckle, 1991). Both these elements are more soluble under acidic conditions. In plants, B and Zn concentrations are usually in the range of 10–50 mg kg^{-1} and 20–100 mg kg^{-1}, respectively.

The spatial distribution of soil contaminants is usually heterogeneous, not only over scales of metres and beyond, but also at smaller scales. The heterogeneous distribution of soil contaminants affects root growth. The roots of some tree species avoid hotspots contaminated with heavy metals (Dickinson *et al*., 1991; Breckle & Kahle, 1992). Conversely, roots of the Zn hyperaccumulator *Thlaspi caerulescens* (J. Presl & C. Presl) actively forage Zn-rich hotspots in soils (Schwartz *et al*., 1999; Whiting *et al*., 2000).

The response of roots to heterogeneously distributed soil contaminants may profoundly affect their uptake by plants as well as their leaching into receiving waters. The underlying principles of how heterogeneously distributed trace elements influence plant root growth are not well understood. In order to reveal such mechanisms, it is important to visualize root growth and activity with minimum disturbance.

The aim of this study was to elucidate the potential of NR to monitor root growth in heterogeneously contaminated media. For this purpose, we chose to investigate the growth of lupin (*Lupinus albus* L.) in soil heterogeneously contaminated with B and Zn.

Materials and methods

Neutron radiography system

The experiment was performed at the Neutron Radiography facility (NEUTRA) at the Paul Scherrer Institute (PSI), Villigen, Switzerland (Lehmann *et al*., 2001). This facility consists of a neutron source, collimator, sample, and image detector. The neutron-generating source can be a reactor, the target of an accelerator, or a neutron-emitting isotope. The NEUTRA facility at PSI uses neutrons emitted from a lead (Pb) target that is bombarded with high-energy protons. A heavy-water moderator then converts high-energy neutrons into thermal neutrons.

The collimator is a beam-forming assembly that determines the geometric properties of the beam and contains filters that reduce the intensity of gamma rays. The image resolution depends on the collimator geometry and is expressed by the collimation ratio L/D, where L is the collimator length and D is the diameter of the inlet aperture of the collimator on the side facing the source. In our study, a neutron flux of 3×10^{10} m^{-2} s^{-10} was used with a mean energy of 25 meV and a collimation ratio of $L/D = 550$. The beam was transmitted through the sample and a plane position-sensitive detector recorded the resulting image. This detector records a two-dimensional image that is a projection of the object on the detector plane. We used a CCD camera detector with an array of 1024 × 1024 pixels, giving a resolution of 110–270 μm in the digital images.

Material testing

We grew the plants in quartz sand and a natural soil (loamy sand). Sand and soil samples were prepared in slab-shaped aluminium containers because of the transparency (poor attenuation) of aluminium to neutrons. We used slabs with inner dimensions of 0.17 × 0.15 × 0.013 m (Figure 1). Preliminary tests revealed that a slab thickness of 0.013 m gave good contrast in the images, while providing adequate space for root development.

Experiment 1

Quartz sand. Two slabs were filled with acid-washed dry quartz sand, with grain size of 100–500 μm. The average bulk density of the packed sand was 1.8 Mg m^{-3}. A single lupin seed was sown directly onto the surface at the centre of the slabs. The plants were grown in a controlled environment chamber at 21/16°C (day/night), a daily photoperiod of 16 hours, with fluorescent lighting (9000–10 000 Lux), for 10 days before first imaging.

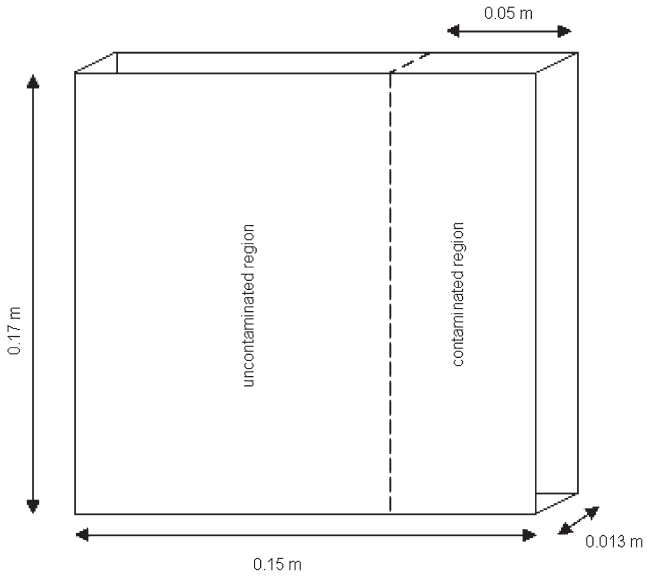

Figure 1 Experimental design of the heterogeneously contaminated slabs.

The sand slabs were irrigated with Hoagland's nutrient solution with a pH of 6.

Loamy sand field soil. Three slabs were prepared with an acidic loamy sand soil (Haplic Alisol), which was obtained from a site along the River Rhine under mixed deciduous forest in the vicinity of Zurich, Switzerland (87% sand, 8% silt, 5% clay; pH = 4.2; organic carbon = 3.2 g kg^{-1}; bulk density = 1.4 Mg m^{-3}). The plants were grown in the controlled environment chamber for 2 weeks before the first imaging. Soil slabs were irrigated with tap water.

During the imaging period, planted slabs were not removed from the NEUTRA facility for safety reasons. Fluorescent lighting and air conditioning maintained a day/night temperature of 21/16°C and a daily photoperiod of 16 hours. Images of the sand slabs were taken weekly for a period of 4 weeks. In the soil slabs, we stopped imaging after the third week due to a faster root growth, which had filled the entire soil volume of the slabs.

Experiment 2

Based on the results of Experiment 1, which proved soil to be a better growing medium, we selected the loamy sand for further experiments. In order to determine a suitable level of contamination to be applied in the imaging experiment, we performed two pot experiments using soils spiked with B and Zn to study the growth of lupin (*Lupinus albus* L.), maize (*Zea mays* L.), poplar (*Populus tremula* L.), willow (*Salix viminalis* L.) and mustard (*Brassica juncea* L.). The loamy sand soil was mixed with 0, 6, 12, 25, 50 and 100 mg B kg^{-1} and 0, 125, 250, 500, 1000 and 2000 mg Zn kg^{-1}. We found that concentrations between 6 and 25 mg kg^{-1} B and 125 mg kg^{-1} Zn were sufficient to induce toxicity symptoms in leaves of lupin, yet not result in plant death.

Experiment 3

Based on the results of Experiment 2, we chose three treatments: two concentrations of B (10 and 20 mg kg^{-1}) and one concentration of Zn (100 mg kg^{-1}) for further investigation. We

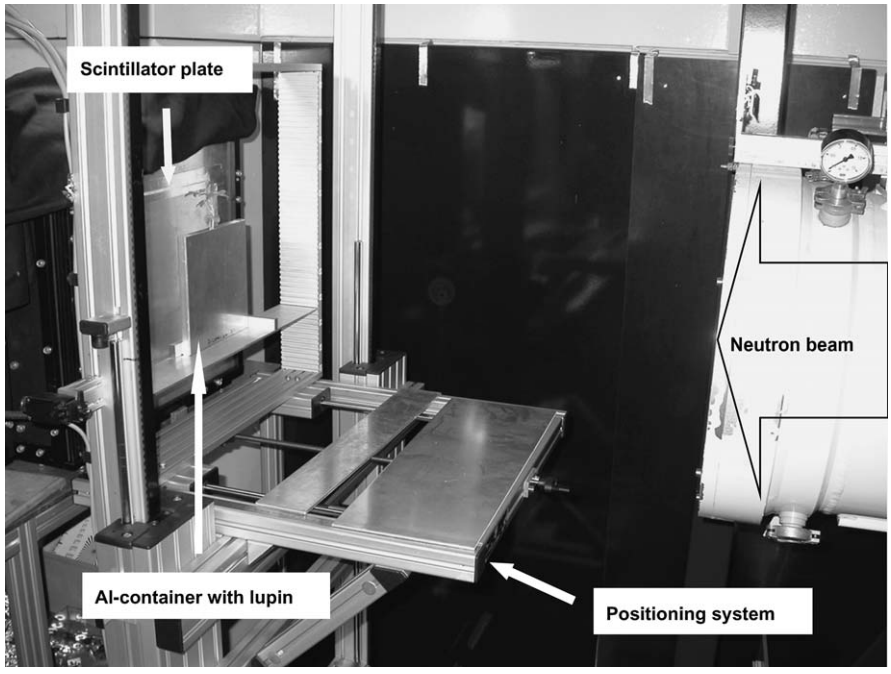

Figure 2 The neutron imaging set up during the experiment. The position of the sample was adjusted using a calibrated positioning system.

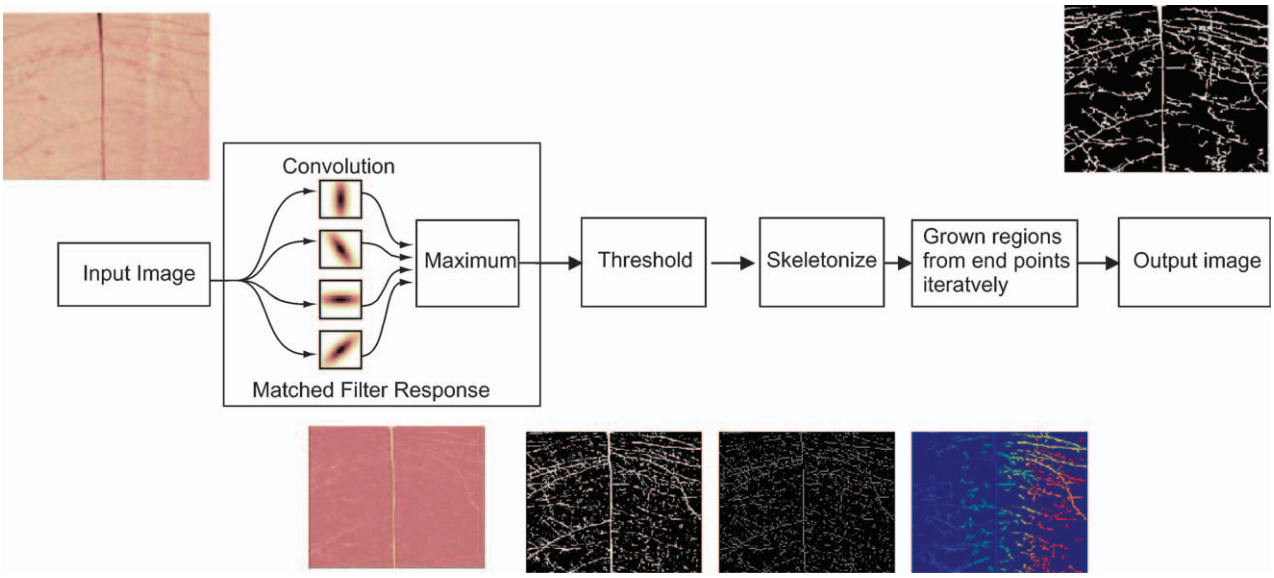

Figure 3 Schematic description of Hoover's blood vessel segmentation method proposed by Hoover *et al.* (2000).

prepared three replicates of slabs with the control soil, homogeneously contaminated soil, and heterogeneously contaminated soil. The treatment levels were achieved by mixing H_3BO_3 or $ZnCl_2$ into the loamy sand soil.

The heterogeneously contaminated slabs consisted of two vertical bands: a 0.05-m contaminated zone, and a 0.10-m uncontaminated zone (Figure 1). Controls were prepared with uncontaminated soil only. Three replicates were prepared for each treatment. The final bulk density of the soil was 1.4 Mg m^{-3}. The slabs were initially saturated with water to allow settling of the soil. In each slab, one seed was sown in the centre, i.e. in the uncontaminated zone. Plants were irrigated every second day to maintain water content at around 25% (–3.7 kPa). After 2 weeks in the above-mentioned growth chamber, the slabs were transferred to the NR facility for imaging. At the conclusion of the experiment, the slabs were opened and the root mass was measured directly. For the heterogeneously contaminated soil, the slabs were opened at one side and the soil cut into six segments (0.075 m × 0.05 m), and each individual segment carefully removed. Roots were separated from the soil with a 2-mm mesh sieve. After washing and drying, the biomass of the roots was obtained for each individual segment.

Imaging procedure

The images were taken at least 2 days after irrigation to decrease the heterogeneity of the water distribution in the slab. This optimized the root-soil contrast at the time when the images were taken, without subjecting the plants to severe water stress. Samples were moved to the NEUTRA imaging system and fixed in the same position each time using a three-dimensional positioning system Figure 2). This consistent placement was important for the comparison of subsequent images.

We used exposure times of 60 s and 20 s per image for the sand slabs and soil slabs, respectively. These exposure times gave the best signal-to-noise ratio and allowed the differentiation of the main roots from the porous medium. To correct variations of the beam intensity over the image area, we collected open beam images without a sample as well as background images, with neither sample nor beam. The neutron radiation dose received

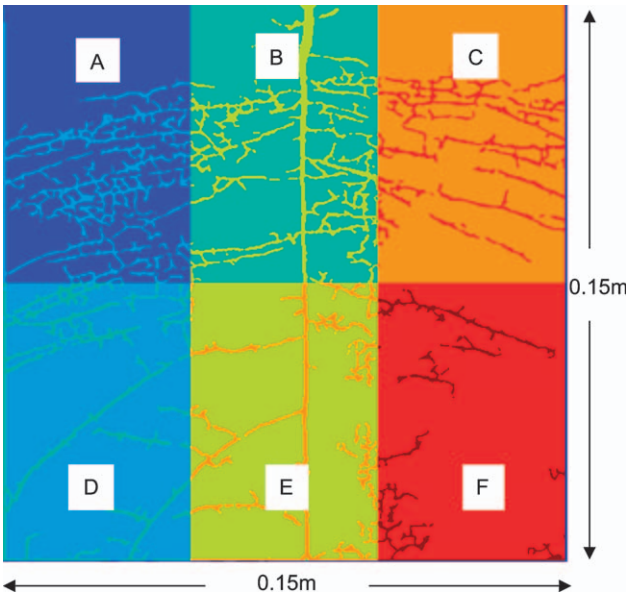

Figure 4 Image regions for volume estimation that correspond to the segments from heterogeneously contaminated soil slabs.

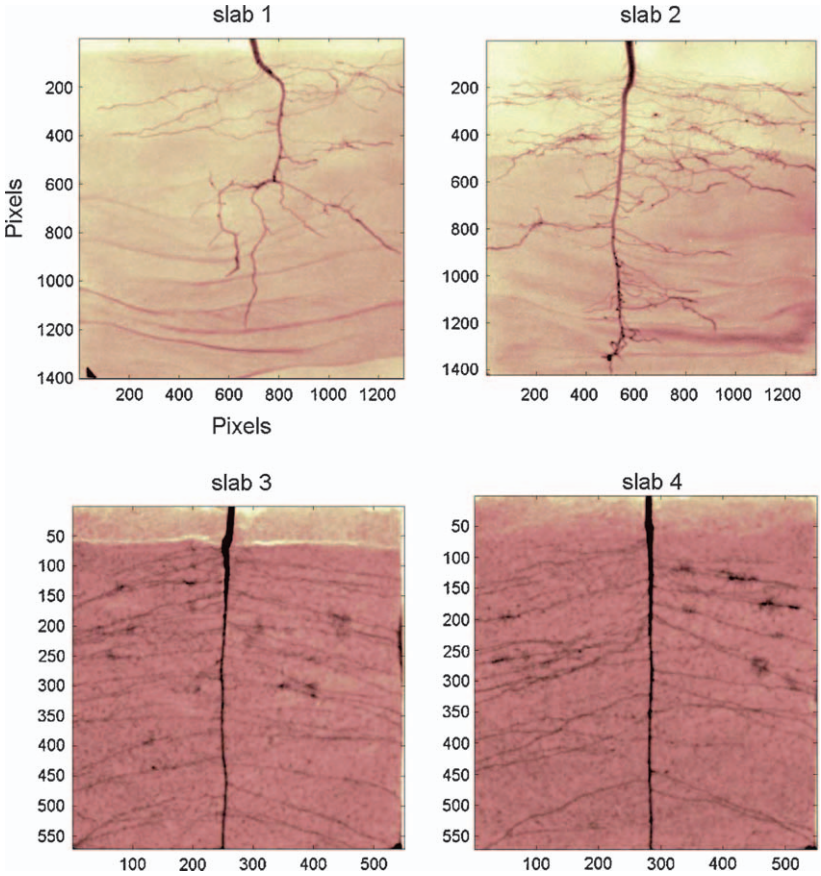

Figure 5 Comparison of root growth in quartz sand (slabs 1 and 2) and field soil media (slabs 3 and 4). The slabs have dimensions of 0.15 m × 0.15 m. Greater pixel values indicate greater resolution.

by these plants was about 0.003 mSv hour^{-1}, some two orders of magnitude less than the minimum value of 0.2 mSv hour^{-1} required to affect plant growth (Real *et al*., 2004).

Image analysis

The radiography images that show the neutron shadow of the sample were first corrected for beam variations and camera noise using a flat field correction:

$$I' = \frac{I_{\text{raw}} - I_{\text{dark}}}{I_{\text{openbeam}} - I_{\text{dark}}}. \quad (2)$$

This operation is done pixel-wise, where I_{raw} is the image as registered by the camera, I_{dark} is the dark noise image without the beam, and I_{openbeam} contains the spatial field variation of the beam without object. A normalization factor, N, is required so that the resulting image data are in the valid dynamic range for a 16-bit TIFF format. This permits the optimal visualization of the data and facilitates quantification. The negative logarithm of the corrected image intensities, I', was used to extract the information with Equation (1). The resulting image was analysed further to differentiate roots from surrounding media. This was achieved by segmentation of the root network.

The background grey-level intensity within each image varied so much that a single global threshold could not segment the roots satisfactorily, i.e. the grey-level of roots in one part of the image was the same as the background in another part. Hoover *et al*. (2000) developed an algorithm for segmenting blood vessels in retinal images that had similar characteristics to ours. Hoover's segmentation method consists of several steps, as described schematically in Figure 3. The first step is to enhance the root contrast using a matched filter response (MFR) image (Chaudhuri *et al*., 1989). The MFR image is computed pixel-wise by selecting the maximum response from a set of images filtered by a bank of oriented Gaussian convolution kernels. The intensity variations in the MFR image are flattened. Next, a threshold of between 80% and 97.5% of the pixels in the MFR image are labelled as background. The percentage depends on the size of the root network. This pre-segmented image is then skeletonized with a thinning algorithm (Lam *et al*., 1992).

The final initialization step before the region-growing iterations is to remove branch points in the skeleton and to identify the end-points. The skeleton end-points are used as seeds for region growing. The region growing acts locally on pieces connected to the end-points, where all pixels with a grey-level greater than the end-point are added to the piece.

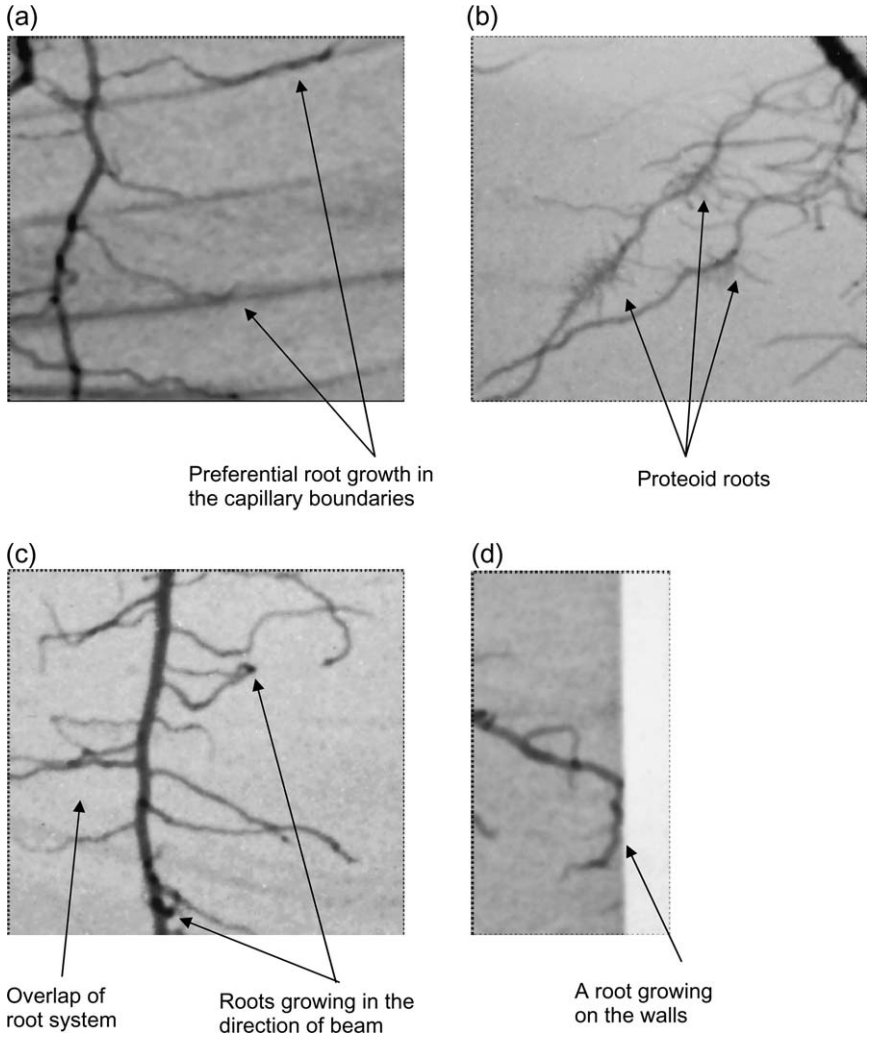

Figure 6 Additional features observed from the images, in each case zooming into a 0.04 m × 0.04 m region. (a) Preferential root growth in the capillary boundaries; (b) proteoid roots; (c) dark spots, which result from root growth in the direction of beam or overlap of roots; and (d) wall effects (0.02 m × 0.04 m).

When all pixels for a given level are collected, a number of shape tests are made. When all tests are positive, the threshold level is decremented and a new iteration is started. If, on the other hand, one of the structure tests fails the threshold probing, then the iteration will be terminated. In order to be labelled as a root segment, the piece must not exceed given size criteria. The skeleton end-points of accepted pieces are added to the list of end-points and the main iteration loop is repeated. The end-points of the accepted pieces are added to the list of end-points. The iteration procedure is repeated until there are no end-points left to segment.

We calculated root volumes using the Euclidean distance map and the skeleton of the segmented roots. We assumed that a large number of cylinder segments with the radius taken as the distance for each skeleton pixel would approximate to the root volume. The cylinder height was defined as the pixel resolution. The total volume, V (m^3), can thus be described as:

$$V = \pi k^3 \sum_{p \in g_{SK}} g_{Dist}(p)^2, \quad (3)$$

where g_{Dist} is the distance map of the segmented image g, g_{SK} is the skeleton of it, the constant k is the side length of a pixel (m), and p represents the pixels of the skeleton. In our investigation, we did not compute the volume for the whole image but rather the six segments of the image, as shown in Figure 4.

Results and discussion

Comparison of root growth in quartz sand and soil

Figure 5 shows the NR images of root development in the quartz sand after 17 days and soil slabs after 14 days. The contrast and resolution were excellent, particularly in the sand slabs. The

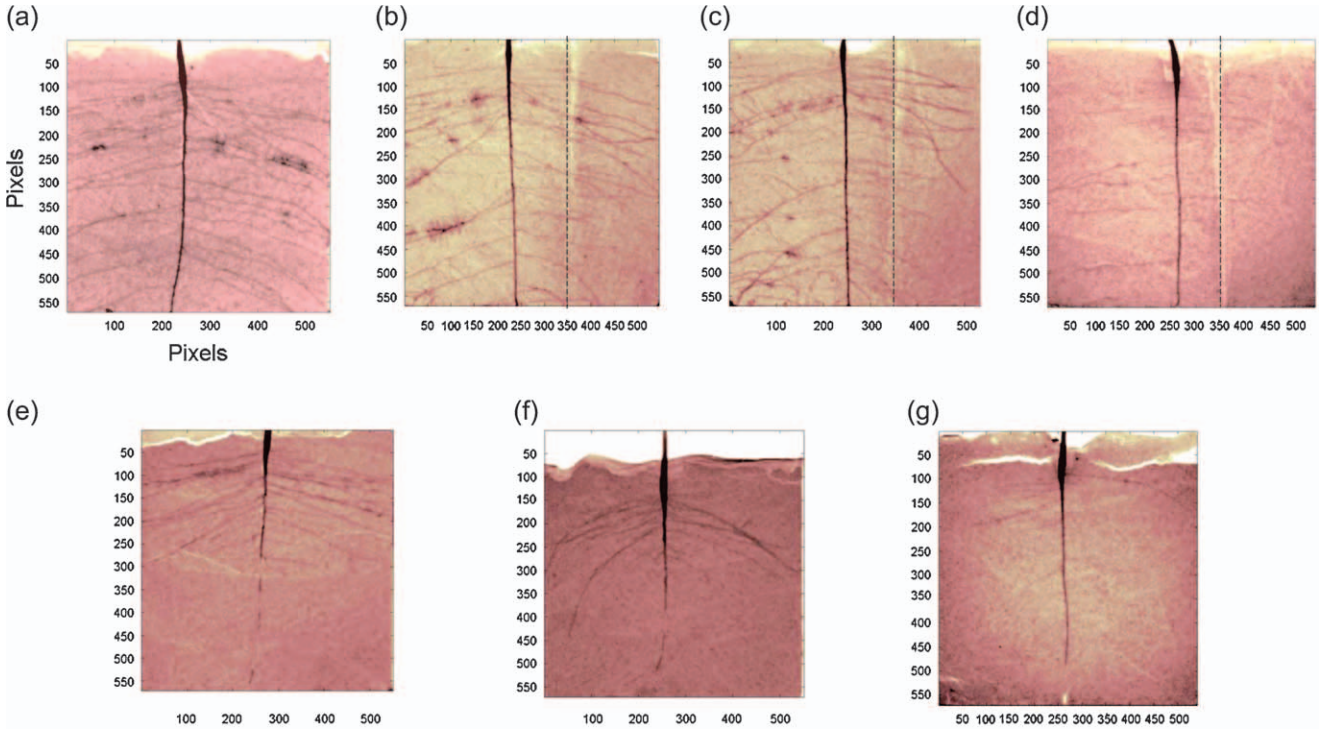

Figure 7 Root growth patterns in slabs: (a) control; (b) heterogeneously contaminated with 10 mg B kg^{-1}; (c) with 20 mg B kg^{-1}; (d) with 100 mg Zn kg^{-1}; (e) fully contaminated with 10 mg B kg^{-1}; (f) with 20 mg B kg^{-1}; and (g) with 100 mg Zn kg^{-1}. The slabs have dimensions of 0.15 m × 0.15 m.

sand slabs showed thin horizontal bands of greater moisture content, which results from the capillary-barrier effect of thin beds of coarser sand particles underlying beds of finer sand. The roots can be clearly distinguished from these bands by their continuity and orientation (Figure 5a,b).

The root-soil contrast was less in the slabs filled with soil than in the quartz sand. Nevertheless the roots were sufficiently visible to determine their growth pattern (Figure 5c,d). Roots grew much faster in the soil slabs than in the quartz sand. After 14 days, the tap root and the laterals had reached the edges of the containers filled with soil, whereas in sand this was achieved only after 24 days of growth. Furthermore, tap roots were straighter and longer in the soil than in the sand slabs, where roots were more twisted and shorter. In the soil, the laterals branched off in a more regular pattern, grew thicker and followed a rather straight, slightly oblique direction downwards, while in the quartz sand they were more fibrous and spread out. The bulk density of the quartz sand (1.8 Mg m^{-3}) was much greater than the soil (1.4 Mg m^{-3}). This was the likely reason for the reduced root penetration, which resulted in a more-branched root system. Therefore, we conclude that although quartz sand provided better quality images than field soil, its use for studying root growth patterns is limited because it impedes root growth.

An additional problem with using quartz sand was the separation of the size-fractions when filling. The roots grew preferentially along the bands of fine sand that had relatively greater moisture content (Figure 6a). This shows the potential of NR to monitor variations in the distribution of soil moisture simultaneously with root growth, but creates an extra complication when investigating other phenomena.

The development of proteoid roots was another feature recognizable in many images (enlarged in Figure 6b). This was observed in both quartz sand and soil slabs, but with poorer resolution in the latter. Proteoid roots, also called cluster roots, are stout bottle-brush-like clusters of rootlets. They arise from the pericycle opposite the protoxylem poles along the lateral roots in many plant families (Neumann & Martinoia, 2002).

The visibility of roots in NR images depends on their orientation. Roots that grow in the direction of the beam only appear as darker pixels (Figure 6c), because the beam in transmission has a greater amount of water to penetrate and is thus attenuated more strongly. Similarly, darker spots occur where two roots overlap or cross each other. The images demonstrate that the thickness of the porous medium was sufficient to allow growth in all directions. There was enough space for lateral roots to cross each other.

The images further show how roots react when they reach container walls and at about what time this occurred. After 4 weeks only a few roots had just reached the walls, while a few days later the development of the root system was strongly influenced

by this space limitation (Figure 6d). This limitation is a principle problem in pot experiments, as roots start to coil around the walls of the containers within a short time. NR allows us to monitor the distance of root tips to the container wall and to determine when they reach the walls. This may provide valuable information for planning and interpretation of pot experiments.

Root growth under B and Zn contamination

The spatial distribution of B and Zn affected lupin root growth. Figure 7 shows the clearest images obtained for all treatments. Significantly fewer roots were produced in homogeneously contaminated slabs compared with the control slabs (Figure 7a). In the heterogeneously contaminated slabs, lateral roots initially grew into the contaminated zone. However, as the plants developed root growth was inhibited in the contaminated zone (Figure 7b,c,d). This trend occurred in all heterogeneously contaminated slabs.

A significant reduction in dry shoot and root biomass was observed in all homogeneously contaminated slabs compared with both control and heterogeneously contaminated soils for both B and Zn treatments. In the Zn treatments, shoot and root weights were significantly reduced in the heterogeneously contaminated slabs (Figure 8). The percentage of roots (ratio of root weight in each segment to the total root weight) was significantly reduced in all contaminated portions of these slabs (Table 1). The smallest percentage of roots was observed in the lower part of the contaminated zones ('F' zone in Table 1). Computed root volumes from the heterogeneously contaminated slabs were related logarithmically to the measured percentage of roots (Figure 9). However, at values above 1% of the total root volume, this relation could be approximated by a linear regression. The systematic error at smaller root volumes is the result of the algorithm overestimating roots with a diameter less than three pixels (450 μm). Such errors will be reduced as improvements in measurement technology allow a picture of the root at finer resolution.

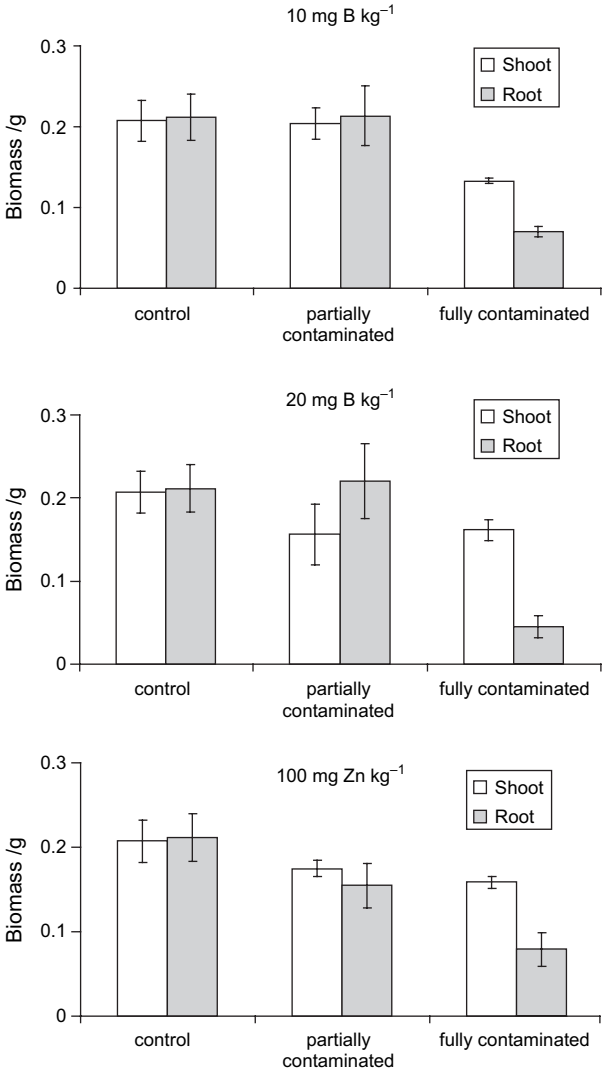

Figure 8 Average shoot and root biomass in control, heterogeneously (partially contaminated) and fully contaminated (fully contaminated) slabs. Error bars are standard errors of the mean ($n = 3$). Means with non-overlapping error bars are significantly different at the 5% level.

Conclusions

Neutron radiography is an effective tool for the non-destructive investigation of root growth. Although sand provided better contrast of roots than real soil, the root growth was significantly perturbed. Root growth in soil gave sufficient contrast to elucidate the decreased growth in the zones contaminated with B or Zn. Testing new materials under different conditions combined with new image processing techniques will doubtless lead to improved image contrast.

Table 1 Each heterogeneously contaminated slab was divided into six segments of 0.075 m × 0.05 m named from A to F (see Figure 4). The table shows the average percentage of roots in each segment of these slabs. Sections A, B, D and E were uncontaminated, while C and F were contaminated

	Concentration of B and Zn in the contaminated segment zones		
Segments	10 mg B kg^{-1}	20 mg B kg^{-1}	100 mg Zn kg^{-1}
A	12.84 ± 1.72*	10.96 ± 3.58	15.67 ± 13.56
B	52.48 ± 11.57	48.78 ± 1.46	41.18 ± 15.13
C	7.43 ± 1.96	10.74 ± 1.89	6.88 ± 5.45
D	15.03 ± 6.63	17.90 ± 5.58	20.24 ± 4.22
E	9.93 ± 4.15	10.36 ± 1.46	15.50 ± 7.88
F	1.85 ± 0.43	1.15 ± 0.54	0.50 ± 0.50

*Standard error; $n = 3$.

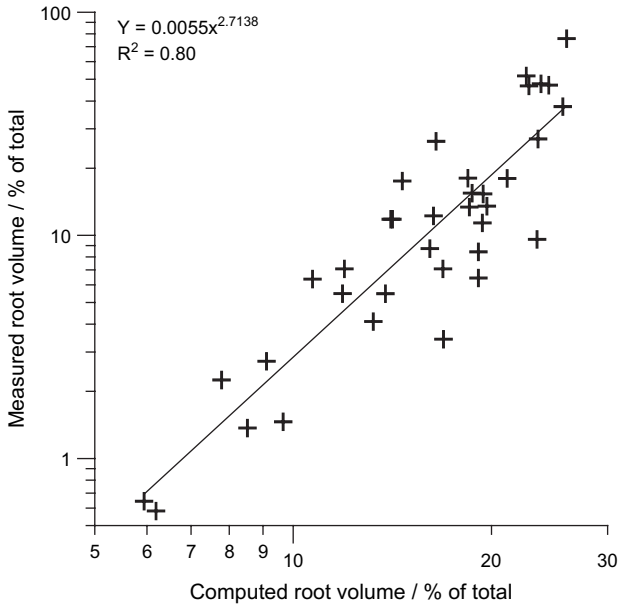

Figure 9 The relationship between the computed root volume and measured root weight, as a percentage of the total, in the heterogeneously contaminated slabs.

Acknowledgements

This study was funded by the Swiss National Science Foundation. We highly appreciate the technical support from Mr H. Laeser of the Institute of Terrestrial Ecology, ETH, and Mr P. Vontobel and Mr S. Hartmann of the Paul Scherrer Institute.

References

Breckle, S.W. 1991. Growth under stress: heavy metals. In: *Plant Roots: the Hidden Half* (eds Y. Waisel, A. Eshel & U. Kafkafi), pp. 351–373. Marcel Dekker, New York.

Breckle, S.W. & Kahle, H. 1992. Effects of toxic heavy-metals (Cd, Pb) on growth and mineral nutrition of beech (*Fagus sylvatica* L.). *Vegetatio*, **101,** 43–53.

Chaudhuri, S., Chatterjee, S., Katz, N., Nelson, M. & Goldbaum, M. 1989. Detection of blood vessels in retinal images using two-dimensional matched filters. *IEEE Transactions on Medical Imaging*, **8,** 263–269.

Couchat, P., Moutonnet, P., Houelle, M. & Picard, D. 1980. *In situ* study of corn seedling root and shoot growth by neutron radiography. *Agronomy Journal*, **72,** 321–324.

Dickinson, N.M., Turner, A.P. & Lepp, N.W. 1991. Survival of trees in a metal-contaminated environment. *Water, Air and Soil Pollution*, **57,** 627–633.

Furukawa, J., Nakanishi, T.M. & Matsubayashi, H. 1999. Neutron radiography of a root growing in soil with vanadium. *Nuclear Instruments and Methods in Physics Research. Section A: Accelerators, Spectrometers, Detectors and Associated Equipment*, **424,** 116–121.

Gregory, P.J., Hutchison, D.J., Read, D.B., Jenneson, P.M., Gilboy, W.B. & Morton, E.J. 2003. Non-invasive imaging of roots with high resolution X-ray micro-tomography. *Plant and Soil*, **255,** 351–359.

Hoover, A., Kouznetsova, V. & Goldbaum, M. 2000. Locating blood vessels in retinal images by piecewise threshold probing of a matched filter response. *IEEE Transactions on Medical Imaging*, **19,** 203–210.

Kasperl, S. & Vontobel, P. 2005. Application of an iterative artefact reduction method to neutron tomography. *Nuclear Instruments and Methods in Physics Research. Section A: Accelerators, Spectrometers, Detectors and Associated Equipment*, **542,** 392–398.

Lam, L., Lee, S.W. & Suen, C.Y. 1992. Thinning methodologies: a comprehensive survey. *IEEE Transactions on Pattern Analysis and Machine Intelligence*, **14,** 869–885.

Lehmann, E.H., Vontobel, P. & Wiezel, L. 2001. Properties of the radiography facility NEUTRA at SINQ and its potential for use as a European reference facility. In: *Proceedings of Sixth World Conference on Neutron Radiography, Osaka, Japan* (eds S. Fujine, H. Kobayashi & J.P. Barton), p. 151. Gordon & Breach Science Publishers, USA.

Majdi, H. 1996. Root sampling methods: applications and limitations of the minirhizotron technique. *Plant and Soil*, **185,** 255–258.

Neumann, G. & Martinoia, E. 2002. Cluster roots: an underground adaptation for survival in extreme environments. *Trends in Plant Science*, **7,** 162–167.

Pierret, A., Kirby, M. & Moran, C. 2003. Simultaneous X-ray imaging of plant root growth and water uptake in thin-slab systems. *Plant and Soil*, **255,** 361–373.

Real, A., Sundell-Bergman, S., Knowles, J.F., Woodhead, D.S. & Zinger, I. 2004. Effects of ionising radiation exposure on plants, fish and mammals: relevant data for environmental radiation protection. *Journal of Radiological Protection*, **24,** A123–A137.

Schwartz, C., Morel, J.L., Saumier, S., Whiting, S.N. & Baker, A.J.M. 1999. Root development of the zinc-hyperaccumulator plant *Thlaspi caerulescens* as affected by metal origin, content and localisation in soil. *Plant and Soil*, **208,** 103–115.

Whiting, S.N., Leake, J.R., McGrath, S.P. & Baker, A.J.M. 2000. Positive responses to Zn and Cd by roots of the Zn and Cd hyperaccumulator *Thlaspi caerulescens*. *New Phytologist*, **145,** 199–210.

Willatt, S.T. & Struss, R.G. 1978. Germination and early growth of plants studied using neutron radiography. *Annals of Botany*, **43,** 415–422.

Willatt, S.T., Struss, R.G. & Taylor, H.M. 1978. *In situ* root studies using neutron radiography. *Agronomy Journal*, **70,** 581–586.